Progress In Electromagnetics Research C, Vol. 26, 83–95, 2012

BROADBAND CPW-FED CIRCULARLY POLARIZED ANTENNA WITH EQUIANGULAR TAPERED-SHAPED FEEDLINE FOR ULTRA-WIDEBAND APPLICATIONS

Q. Chen*, H.-L. Zheng, T. Quan, and X. Li

National Laboratory of Antennas and Microwave Technology, Xidian University, Xi'an, Shaanxi 710071, P. R. China

Abstract—A novel coplanar waveguide (CPW)-fed circularly polarized (CP) antenna is proposed. The antenna is composed of a square ground plane with a circular slot and an equiangular tapered-shaped feedline. With the use of a special shaped feedline, the axial ratio (AR) bandwidth of the proposed antenna is about 61.9% (2.9–5.5 GHz), which is larger than most of similar antennas proposed before. In addition, the impedance bandwidth, determined by 10-dB return loss, is between 2.9–20 GHz, which makes the antenna be used for ultra-wideband (UWB) applications.

1. INTRODUCTION

UWB technology featuring very high-speed data rates, low power consumption and good immunity to multipath effects has become a very promising solution for indoor wireless radio, imaging and radars [1, 2]. Since the rules for the utilization of the 3.1–10.6 GHz unlicensed band for commercial UWB communications were first approved by the Federal Communication Commission (FCC) in 2002 [3], the UWB technology has attracted significant attention and developed rapidly in modern wireless communication. Furthermore, due to the increasing demands for high-quality wireless communication system, CP antennas have been widely used for that they can allow a more flexible orientation between the transmitting and receiving antennas and be less sensitive than linear polarization. In recent years, printed slot antennas have become popular structures to generate CP operation, since they not only have low profile and are easy to be integrated with active devices, but also have larger impedance

Received 6 November 2011, Accepted 4 December 2011, Scheduled 12 December 2011
* Corresponding author: Qiong Chen (chenqiong2100@163.com).

bandwidths compared with microstrip antennas [4, 5]. A CPW-fed square-ring slot antenna was designed by using a T-shaped metallic strip architecture in [6]. The construction, however, is limited with the 3-dB AR bandwidth, which is only 18%. To solve this problem, a novel design of CPW-fed antenna with a lightening-shaped feedline and two inverted-L grounded strips is described in [7] and the AR bandwidth is extended to 48.8%. As similar studies of the CP slot antennas, many other structures have also been proposed in [8–11]. However, most of them can't be used for UWB applications because of the limitation of impedance bandwidths.

In many situations, the impedance and AR bandwidths of the slot antennas are mainly depended on the structures of the antennas' feedlines or stubs. As spiral structures have traveling-wave characteristic and can generate CP operation without the use of other CP techniques [12, 13], they are confirmed promising designs to enhance the bandwidths of slot antennas. In [14], as did the research in early years, a single spiral strip is used in microstrip slot antenna, but both the AR and impedance bandwidths are narrow. In [15], a single-arm equiangular tapered-shaped feedline is introduced and about 30% impedance bandwidth and 20% AR bandwidth are achieved. To further improve the performance, a similar structure of the feedline is applied to a backed-cavity antenna in [16], which is employed to generate a 2×2 array, and the AR and impedance bandwidths can be extended to 50% and 70%, respectively.

In this paper, a novel CPW-fed CP antenna with an equiangular tapered feedline is proposed for UWB applications. In the antenna, a circular slot is etched in the centre of the square ground plane, and a single equiangular tapered feedline which was proposed in [15, 16] is implanted in the slot. By optimizing the dimensions of the structure, wide AR and impedance bandwidths are obtained. Details of the antenna design and the measured results of the constructed prototype are presented and discussed.

2. ANTENNAS DESIGN

The geometry of the proposed CP antenna is shown in Figure 1. As can be seen, the ground plane is printed on a square FR4 substrate with a relative permittivity of $\varepsilon_r = 4.4$ and a loss tangent of $\tan\delta = 0.02$. The length of the substrate is G, and the thickness is h. A circular slot with a diameter of D_s is etched in the ground plane. The circular slot is excited by a 50 Ohms CPW which is composed of a signal strip of width $W_f = 3\,\text{mm}$ and two identical gaps of width $g = 0.35\,\text{mm}$. The equiangular tapered feedline implanted in the slot is used to couple the

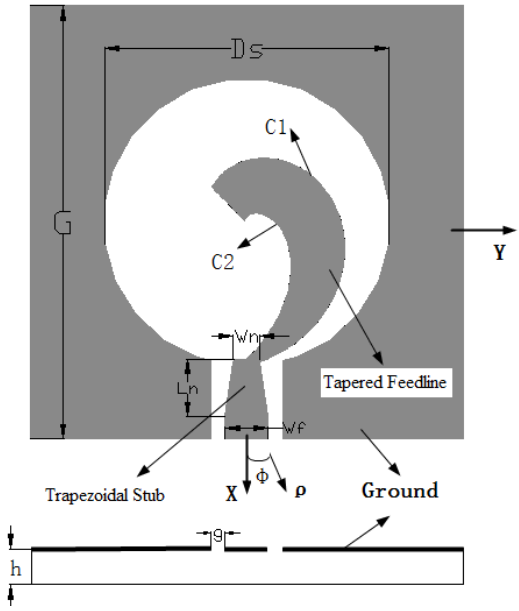

Figure 1. Geometry of the proposed CPW-fed slot antenna with tapered-shaped feedline. Antenna parameters: $G = 60\,\text{mm}$, $D_s = 40\,\text{mm}$, $W_n = 1\,\text{mm}$, $L_n = 10\,\text{mm}$, $W_f = 3\,\text{mm}$, $g = 0.35\,\text{mm}$, $h = 1.6\,\text{mm}$, C_1: $\rho = R_a e^{-a\Phi}$, $\Phi = [0, \Phi_0]$, C_2: $\rho = R_b e^{-b\Phi}$, $\Phi = [0, \Phi_0]$, where $a = 0.27$, $b = 1$ and $\Phi_0 = 1.25\pi$.

electromagnetic energy into slot area from the feeding point [16]. And it is formed by two exponential curves C_1 and C_2, shown in Figure 1. The equations of the two curves can be expressed in polar coordinates as follows:

$$\begin{cases} C_1: & \rho = R_a e^{-a\Phi}, \quad \Phi = [0, \Phi_0] \\ C_2: & \rho = R_b e^{-b\Phi}, \quad \Phi = [0, \Phi_0] \end{cases}$$

where R_a equals a half of the diameter D_s, i.e., $R_a = \frac{1}{2}D_s$, and R_b is a constant that remains to be optimized. a and b are the shrinking coefficients of curves C_1 and C_2, respectively. Φ_0 is the common ending angle of curve C_1 and C_2. Adjusting the parameter a will lead to a variation of impedance matching performance, while the ending angle Φ_0 has a great effect on CP bandwidth. By applying the structure of equiangular tapered feedline to the CPW-fed antenna, both the CP and impedance bandwidths are much wider than those CPW-fed antennas used other types of feedlines in [6–10]. To make the input impedance of the antenna match the impedance of the input port, a

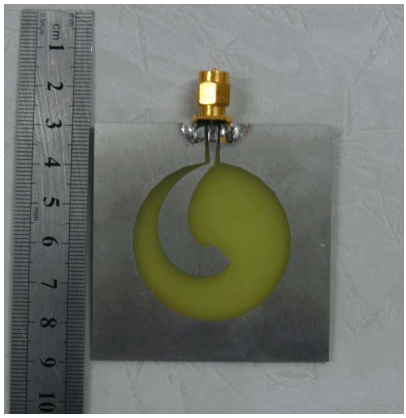

Figure 2. The photograph of the proposed antenna.

trapezoidal turning stub is embedded between the feeding structure and the tapered feedline. As shown in Figure 1, the trapezoid has a height of L_n, a bottom length of W_n and a top length of W_f which equals the width of the signal strip. An appropriate design of the turning stub will much widen the impedance bandwidth.

In addition, the photograph of the manufactured antenna is shown in Figure 2.

3. RESULTS AND DISCUSSIONS

The proposed antenna is simulated by Ansoft HFSS simulation package and measured by Agilent E5071C vector network analyzer. Here, we let $G = 60\,\text{mm}$, $D_s = 40\,\text{mm}$, which are equal to the dimensions of ground plane and slot proposed in [7–11], respectively. Through out the studies presented in this section, all other parameters that haven't been mentioned are fixed to the values shown in Figure 1.

3.1. Mechanism of CP Operation and Impedance Matching

The working principle of CP operation can be demonstrated by time-varying vector magnetic field distributions on the ground plane and feedline. Figure 3 shows the vector magnetic field distributions on the ground plane and the feedline at 4.2 GHz for four different instants, i.e., $w_t = 0°$, $90°$, $180°$ and $270°$. It can be seen that at $w_t = 0°$, as the black color arrow shows, the dominant radiation magnetic field vector is in $+x$ direction. After one quarter period when $w_t = 90°$, the dominant radiation magnetic field vector changes to $+y$ direction. It

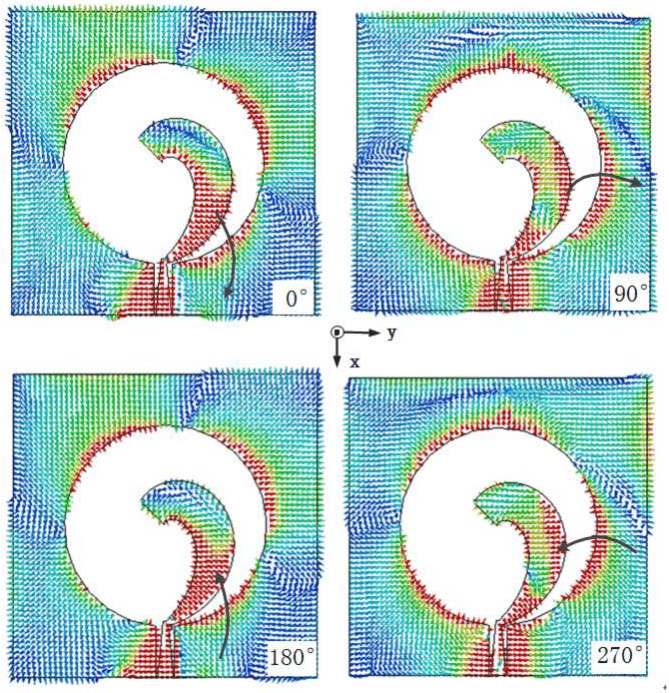

Figure 3. Simulated vector magnetic field distributions at 4.2 GHz.

is noted that the vector magnetic field distributions at $w_t = 180°$ and 270° are equal in magnitude and opposite in phase of $w_t = 0°$ and 90°, respectively. Therefore, it can be concluded that the magnetic field vector rotates in the right-hand direction by 90° in $+z$ direction after a quarter-period, which satisfies the requirement of the spatial and temporal quadrature for circular polarization. As for $-z$ direction, the direction in which the magnetic field vector rotates is opposite to that of $+z$ direction, i.e., the proposed CP slot antenna generates LHCP in $-z$ direction while RHCP in $+z$ direction.

Figure 4 shows the real and imaginary parts of the input impedance and the coefficient reflection S_{11}. As can be seen, the real part of the input impedance slightly fluctuates around 50 Ohms while the imaginary part around 0 Ohm at 2.9–20 GHz. And at 2.9–20 GHz, the coefficient reflection is below -10 dB as Figure 4 shows. That means the antenna has good impedance matching at this frequency band. Considering the traveling-wave structure of the tapered feedline, the input impedance should almost remain stable while frequencies keep increasing. Thus, the impedance matching can be extended to infinite high frequencies.

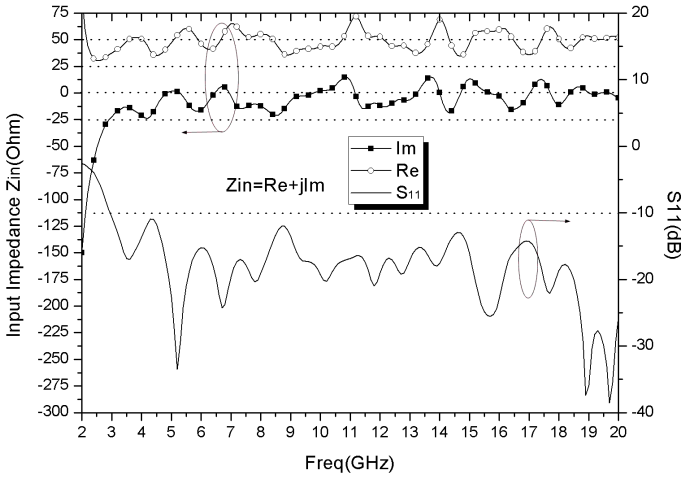

Figure 4. Simulated input impedance varying with frequency.

3.2. Parametric Study of the Performance

Before discussing other parameters, we first study the effect of ground size. In the process of varying the ground-plane size G but fixing the slot size D_s, we have found that the performance of the antenna is very sensitive to the ground-plane size, especially the CP operation. When G is set to 60 mm, equal to the dimension of ground plane proposed in [7–11], the AR bandwidth is 61.9% (2.9–5.5 GHz), and the lower impedance band frequency, defined by the lowest frequency for the reflection coefficient below -10 dB, is 2.9 GHz. If G increases to 65 mm, dual-band CP performance can be achieved, which are 17.5% (2.6–3.1 GHz) and 25.9% (4.2–5.45 GHz), respectively. And the lower band frequency increases to 3.06 GHz. In this situation, the lower CP band 2.6–3.1 GHz is not enclosed by the impedance band(3.06–20 GHz). When G is set to 70 mm, the AR bandwidth decreases to 20.3% (4.2–5.15 GHz) while the lower impedance band frequency increases to 3.15 GHz.

Since several other parameters affect the AR and return loss, here we only discuss about main effect parameters, including shrinking coefficient (a), ending angle (Φ_0) of curves C_1 and C_2, height (L_n) and narrow bottom length (W_n) of trapezoidal turning stub. To simplify the effect of these parameters on the performance, we let R_a and R_b be fixed at its optimism values, which are 20 mm and 19 mm, respectively.

Figure 5 shows the effects of parameter a on the reflection

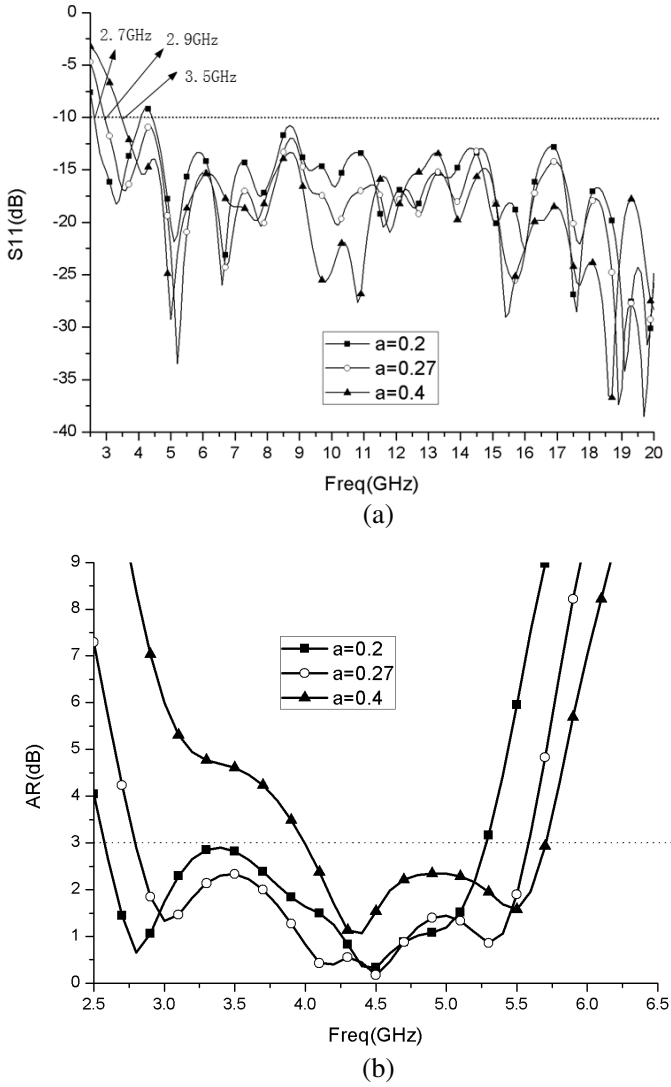

Figure 5. Simulated (a) S_{11} and (b) AR versus frequency for different values of parameter a.

coefficient S_{11} and AR. It is clear that when parameter a increases, the lower band frequency, defined by the lowest frequency for the reflection coefficient below -10 dB, increases. And at higher frequencies, the reflection coefficient remains below -10 dB as a varies. We can also find the CP performance is also effected by a. And a good CP operation

which covers the frequency band of 2.9–5.5 GHz can be attained when $a = 0.27$.

The key point to make sure the antenna radiates CP wave is to properly choose the ending angle Φ_0 [14]. Figure 6 shows the effects of

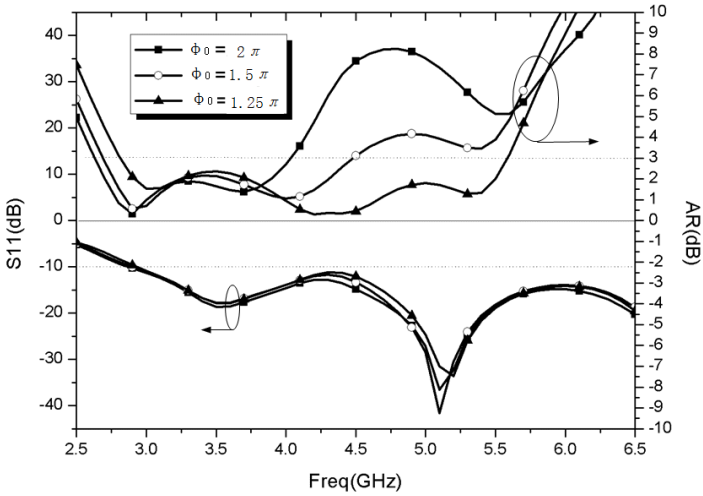

Figure 6. Simulated S_{11} and AR versus frequency for different values of parameter Φ_0.

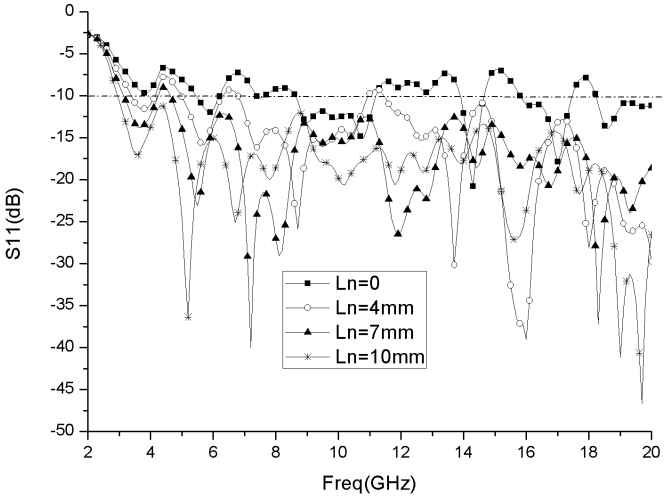

Figure 7. Simulated S_{11} versus frequency for different values of L_n.

ending angle Φ_0 of curves C_1 and C_2 on the performance of the antenna. It can be seen that the S_{11} remains stable when Φ_0 changes. The CP operation at the frequency band of 3.8–5.5 GHz, however, becomes bad as Φ_0 varies from 1.25π to 2π. Best result is attained when $\Phi_0 = 1.25\pi$.

Figure 7 shows the effects of the trapezoidal turning stub on

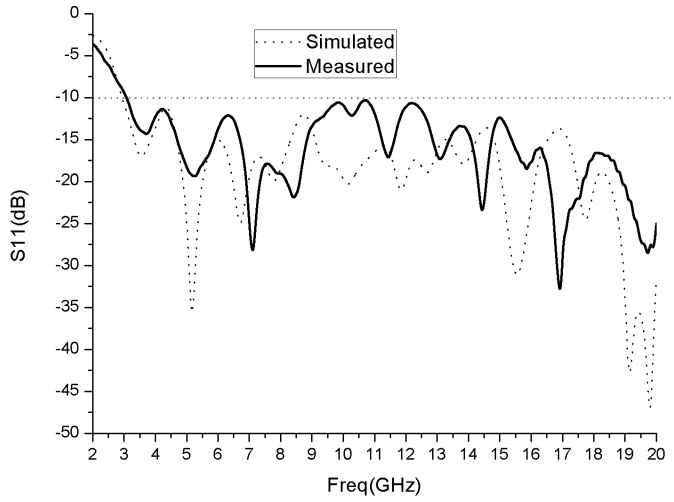

Figure 8. Simulated and measured results of S_{11}.

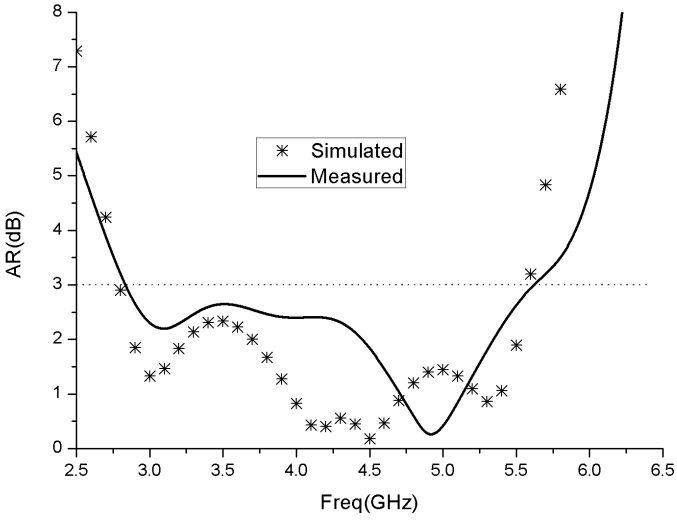

Figure 9. Simulated and measured results of ARs.

the performance of the antenna. W_n is fixed at 1 mm, which is corresponding to 100 Ohms characteristic impedance [17]. As the stub is used to enhance impedance matching, it is only necessary to study its effect on reflection coefficient S_{11}. As Figure 7 shows, the reflection coefficient decreases as L_n increases, and best result is obtained when $L_n = 10$ mm.

3.3. Simulated and Measured Results

Figure 8 shows the measured and simulated results of reflection coefficient at 2–20 GHz. From Figure 8, we can see that at the frequency band of 9–12 GHz, the measured S_{11} performance is not so highly agreement with the simulated results. Besides the fabrication error and the environments of the measurement which may cause this difference, the error occurring during the process of SMA connector

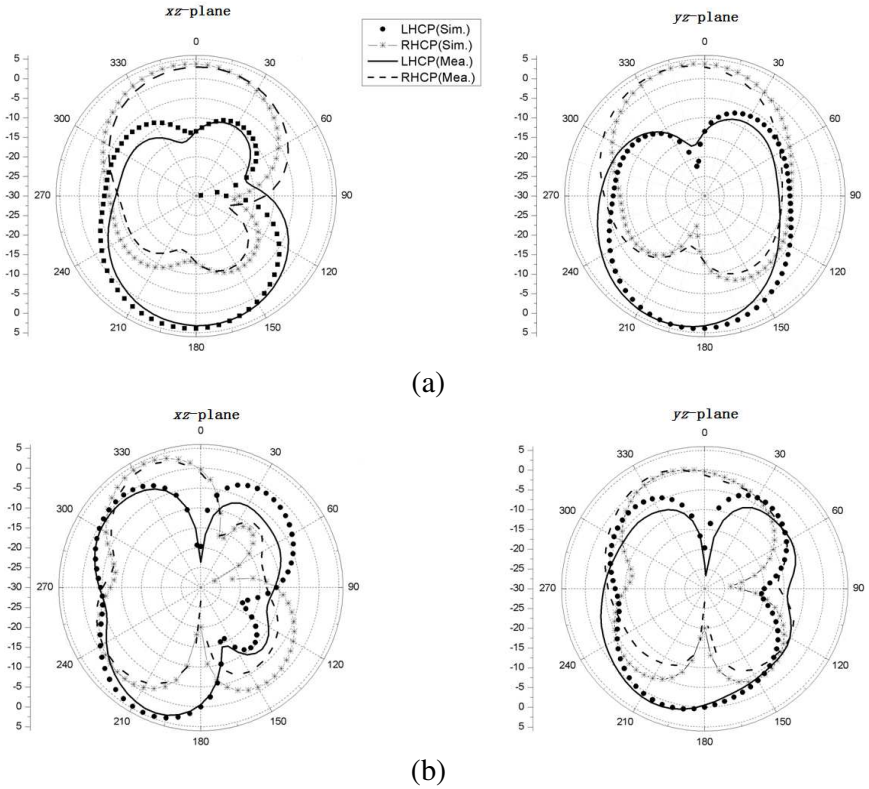

Figure 10. Simulated and measured radiation patterns of the antenna at (a) 3.5 GHz, (b) 5.5 GHz.

(Shown in Figure 2.) being welded will also lead to not so good result of the measured S_{11}. Both the simulated and measured results show the -10 dB impedance bandwidth is about 2.9–20 GHz, and it could include infinite high frequencies as analyzed above.

Figure 9 shows the measured and simulated results of AR. From the two curves, we can know both the measured and simulated results of AR $\leq$ 3 dB at 2.9–5.5 GHz, which means that the AR bandwidth can be up to 61.9%.

Figure 10 shows the measured and simulated radiation patterns at 3.5 GHz and 5.5 GHz. It can be found that the patterns are RHCP for $z > 0$ and LHCP for $z < 0$, which is consistent with the vector magnetic field distribution shown in Figure 3. It also shows that the main beam direction shifts slightly away from the zenith, which is especially apparent at 5.5 GHz. This is because of the asymmetric structure of the antenna. As a result, the main beam direction will shift dramatically from the zenith as the working frequency increases. Figure 11 shows the simulated and measured radiation efficiency and maximum gains of the antenna. The use of low-loss FR4 substrate can lead to a high efficiency at operation band, as can be seen in the figure. Figure 11 also implies that the maximum gains are between 3–5 dBi within the 3-dB AR bandwidth from 2.9 to 5.5 GHz and will remain stable at 7 dBi as the frequency keeps increasing.

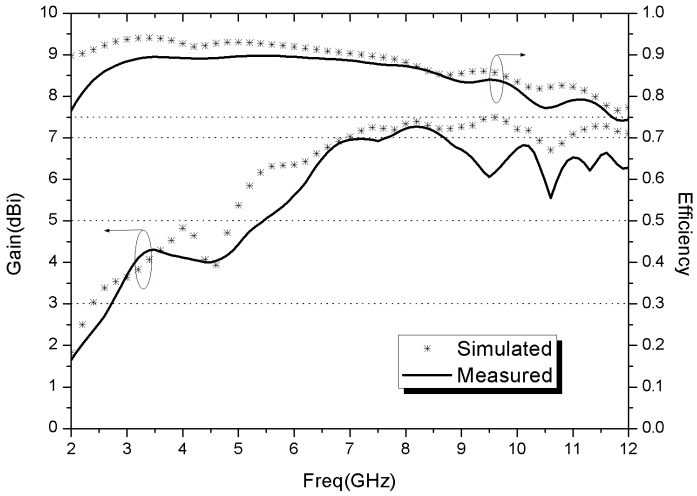

Figure 11. Simulated and measured results of radiation efficiency and maximum gains.

4. CONCLUSION

A CPW-fed CP antenna with ultra-wideband is proposed. The equiangular tapered-shaped feedline consists of two curves protruded from the CPW, and its structure contributes to the generation of CP radiation and UWB characteristic. The trapezoidal turning stub has effectively widened the impedance band. The impedance bandwidth of the proposed antenna is over 2.9–20 GHz (6.7 : 1), and the AR bandwidth is about 61.9% with a range of 2.9–5.5 GHz by the measured results. The maximum gains are about 3–5 dBi within the 3-dB AR bandwidth.

REFERENCES

1. Siwiak, K., "Ultra-wide band radio: Introducing a new technology," *IEEE Veh. Technol. Conf.*, Vol. 2, 1088–1093, May 2001.
2. Leeper, D. G., "Ultra-wideband — the next step in short-range wireless," *IEEE Radio Freq. Integrated Circuits Symp. Dig.*, 493–496, Jun. 2003.
3. "Federal communications commission revision of Part 15 of the Commission's rules regarding ultra-wideband transmission system from 3.1 to 10.6 GHz," Federal Communications Commission, FCC, ET-Docket, 98–153, Washington, DC, 2002.
4. Row, J. S., "The design of a squarer-ring slot antenna for circular polarization," *IEEE Trans. Antennas Propag.*, Vol. 53, 1967–1972, Jun. 2005.
5. Sze, J.-Y., C.-I. G. Hsu, M. H. Ho, Y. H. Ou, and M. T. Wu, "Design of circularly polarized annular-ring slot antennas fed by a double-bent microstrip line," *IEEE Trans. Antennas Propag.*, Vol. 55, 3134–3139, Nov. 2007.
6. Sze, J.-Y., K.-L. Wong, and C.-C. H. Coplanar, "Waveguide-fed square slot antenna for broadband circularly polarized radiation," *IEEE Trans. Antennas Propag.*, Vol. 51, No. 8, Aug. 2003.
7. Sze, J.-Y., C.-I. G. Hsu, Z.-W. Chen, and C.-C. Chang, "Broadband CPW-fed circularly polarized square slot antenna with lightening-shaped feedline and inverted-L grounded strips," *IEEE Trans. Antennas Propag.*, Vol. 58, No. 3, 973–977, Mar. 2010.
8. Liao, W. and Q.-X. Chu, "CPW-FED square slot antenna with lightening-shaped feedline for broadband circularly polarized

radiation," *Progress In Electromagnetics Research Letters*, Vol. 18, 61–69, 2010.

9. Sze, J.-Y. and C.-C. Chang, "Circularly polarized square slot antenna with a pair of inverted-L grounded strips," *IEEE Antennas and Wireless Propagation Letters*, Vol. 7, 2008.
10. Pourahmadazar, J., C. Ghobadi, J. Nourinia, N. Felegari, and H. Shirzad, "Broadband CPW-fed circularly polarized square slot antenna with inverted-L strips for UWB applications," *IEEE Antennas and Wireless Propagation Letters*, Vol. 10, 369–372, May 2011.
11. Felegari, N., J. Nourinia, C. Ghobadi, and J. Pourahmadazar, "Broadband CPW-fed circularly polarized square slot antenna with three inverted-L-shape grounded strips," *IEEE Antennas and Wireless Propagation Letters*, Vol. 10, 2011.
12. Zhang, Y. and L. Zhu, "Printed dual spiral-loop wire antenna for broadband circular polarization," *IEEE Trans. Antennas Propag.*, Vol. 54, No. 1, 284–288, Jan. 2006.
13. Buck, M. and D. Filipovic, "Bi-layer, mode 2, four-arm spiral antennas," *Electron. Lett.*, Vol. 43, No. 6, 1–2, Mar. 2007.
14. Nakano, H., G. Hirokawa, J. Yamouchi, and K. Hirose, "Spiral antenna with coplanar strip line feed," *Electron. Lett.*, Vol. 28, No. 23, 2130–2131, 1992.
15. Hung, K.-F. and Y.-C. Lin, "Simulation of single-arm fractional spiral antennas for millimeter wave applications," *IEEE Antennas and Propag. Society Symposium 2006*, 3697–3700, Jul. 2006.
16. Hung, K.-F. and Y.-C. Lin, "Novel broadband circularly polarized cavity-backed aperture antenna with traveling wave excitation," *IEEE Trans. Antennas Propag.*, Vol. 58, No. 1, Jan. 2010.
17. Balanis, C. A., *Antenna Theory: Analysis and Design*, Wiley, New York, 2005.